Hybrid Nanomaterials

Precisely Size-Tunable Monodisperse Hairy Plasmonic Nanoparticles via Amphiphilic Star-Like Block Copolymers

Yihuang Chen, Young Jun Yoon, Xinchang Pang, Yanjie He, Jaehan Jung, Chaowei Feng, Guangzhao Zhang, and Zhiqun Lin**

In situ precision synthesis of monodisperse hairy plasmonic nanoparticles with tailored dimensions and compositions by capitalizing on amphiphilic star-like diblock copolymers as nanoreactors are reported. Such hairy plasmonic nanoparticles comprise uniform noble metal nanoparticles intimately and perpetually capped by hydrophobic polymer chains (i.e., "hairs") with even length. Interestingly, amphiphilic star-like diblock copolymer nanoreactors retain the spherical shape under reaction conditions, and the diameter of the resulting plasmonic nanoparticles and the thickness of polymer chains situated on the surface of the nanoparticle can be readily and precisely tailored. These hairy nanoparticles can be regarded as hard/soft core/shell nanoparticles. Notably, the polymer "hairs" are directly and permanently tethered to the noble metal nanoparticle surface, thereby preventing the aggregation of nanoparticles and rendering their dissolution in nonpolar solvents and the homogeneous distribution in polymer matrices with long-term stability. This amphiphilic star-like block copolymer nanoreactor-based strategy is viable and robust and conceptually enables the design and synthesis of a rich variety of hairy functional nanoparticles with new horizons for fundamental research on self-assembly and technological applications in plasmonics, catalysis, energy conversion and storage, bioimaging, and biosensors.

1. Introduction

Noble metal nanoparticles often exhibit strong characteristic surface plasmon resonance (SPR) owing to the collective oscillation of conduction electrons when exposing to the external electromagnetic field. They represent an important class of nanomaterials and have attracted much attention for use in biomedical diagnosis and therapy,[1] catalysis,[2] surface-enhanced Raman spectroscopy,[3] etc. In sharp contrast to fluorescent organic dyes which experience photobleaching and degradation during bioimaging, plasmonic nanoparticles (e.g., Au and Ag) possess at least five orders of magnitude larger optical cross-section owing to the surface plasmon enhancement and thus superior photostability.[1] They have also found applications as photothermal therapeutic agents for tumor treatment. Recent research has witnessed rapid advances in rational design and synthesis of plasmonic nanoparticles with controllable and uniform size. They are often achieved by comparatively simple solution-based colloidal synthesis.[4] As nanoparticles tend to aggregate due to their high specific surface area, surface passivation of nanoparticle with ligands (e.g., small molecular surfactants and linear polymers) is of key importance in preventing them from agglomeration. However, the ligands capped on the plasmonic nanoparticle surface are often dynamically stable due to

Y. Chen, Prof. G. Zhang
Faculty of Materials Science and Engineering
South China University of Technology
Guangzhou 510640, China
E-mail: gzzhang@ustc.edu.cn

Y. Chen, Y. J. Yoon, Dr. X. Pang, Y. He, Dr. J. Jung, Dr. C. Feng, Prof. Z. Lin
School of Materials Science and Engineering
Georgia Institute of Technology
Atlanta, GA 30332, USA
E-mail: zhiqun.lin@mse.gatech.edu

DOI: 10.1002/smll.201602820

weak non-covalent binding between ligand and nanoparticle. Thus, the ligand dissociation may occur as experimental conditions (e.g., pH, temperature, UV irradiation, etc.) are changed.[5] Moreover, it remains challenging to utilize small molecular ligand-capped plasmonic nanoparticles for certain applications, for example, surface-enhanced Raman scattering (SERS)-based sensing. The weak interaction between functional groups (e.g., acids and alcohols) in analytes and plasmonic nanoparticles often yield feeble SERS signals due largely to the dynamic adsorption and desorption of attached analytes.[6] Clearly, by employing polymeric ligands, the analytes will likely be encapsulated within the layer of polymeric ligands, thereby leading to the improved SERS.

In this context, several strategies including grafting-from and grafting-to[7] and amphiphilic linear block copolymer micelles[8] have emerged to passivate the surface of nanoparticles with polymer chains as ligands, forming polymer-capped nanoparticles. We note that the grafting-from approach allows for a higher grafting density of polymer chains, and grafting-to approach may suffer from steric hindrance that limits the grafting density. Both approaches may still often encounter the unavoidable association and dissociation of grafted polymers from the nanoparticle surface over a certain period of time, resulting in incomplete and uncontrollable surface coverage or uniformity of polymers on the nanoparticle surface.[9] On the other hand, the size and shape of amphiphilic linear block copolymer micelles formed by self-assembly in the selective solvent depend sensitively on concentration, solvent properties, temperature, pH, etc. Thus, it is difficult to create and maintain strictly structurally stable spherical micelles containing amphiphilic linear block copolymers that can be employed as templates for the growth of nanoparticles.[10–12] A slight variation of experimental conditions noted above could result in nanoparticles with non-uniform size and shape. Clearly, it's highly desirable to develop a versatile synthetic route to strictly size-controlled, homogeneously dispersed and stable nanoparticles with uniform polymer chains perpetually tethered on their surface.

Herein, we report a viable and robust strategy to craft monodisperse plasmonic nanoparticles with precisely tailorable dimensions and compositions intimately and permanently capped with a layer of polymer chains of uniform length (i.e., hairy plasmonic nanoparticles). The key to our strategy is to exploit a set of amphiphilic star-like poly(acrylic acid)-block-polystyrene (PAA-*b*-PS) diblock copolymers with well-defined molecular weights as nanoreactors (i.e., templates) that are rationally designed and synthesized via a sequential atom transfer radical polymerization (ATRP) of *tert*-butyl acrylate (*t*BA) and styrene (St) from a *β*-cyclodextrin-based macroinitiator, followed by the hydrolysis of inner poly(*tert*-butyl acrylate) (P*t*BA) blocks. The precursors are selectively partitioned in the space occupied by the inner hydrophilic PAA blocks of star-like PAA-*b*-PS diblock copolymers. The strong coordination interaction between the carboxylic acid groups of PAA blocks and the metal moieties of Au and Ag precursors lead to the nucleation and growth of PS-capped Au and PS-capped Ag nanoparticles, respectively. Unlike the dendrimer-encapsulated nanoclusters,[13] the diameters of plasmonic Au and Ag nanoparticles and the thickness of outer hydrophobic PS blocks on the nanoparticle surface can be conveniently tailored by varying the molecular weights of inner PAA blocks and outer PS blocks during the ATRP of *t*BA and St, respectively. It is worth noting that our nanoreactor strategy for creating polymer-capped nanoparticles differs significantly from the approaches noted above. First, in stark contrast to copious past works on nanoparticles synthesized from the conventional linear block copolymer micelles, our strategy enables the effective synthesis of monodisperse nanoparticles due to the unimolecular micellar structure of amphiphilic star-like block copolymers. The integrity (i.e., size and shape) of amphiphilic star-like block copolymer templates remain during the reaction owing to their star-shaped nature (i.e., each PAA-*b*-PS diblock "hair" connected to a *β*-cyclodextrin core).[14,15] Second, the polymer "hairs" are permanently anchored on the nanoparticle surface, thus eliminating the aggregation of nanoparticles and imparting their superior solubility and long-term stability in nonpolar solvents and homogeneous distribution in polymer matrices. Conceptually, this amphiphilic star-like block copolymer nanoreactor-based strategy opens the possibility for synthesis of a large variety of hairy functional nanoparticles with accurate control over the size of nanoparticles, length of polymeric ligands, surface chemistry of nanoparticles, and solubility and long-term stability of nanoparticles.

2. Results and Discussion

Scheme 1 depicts the synthetic route to hairy noble metal nanoparticles (i.e., PS-capped plasmonic nanoparticles) by capitalizing on amphiphilic unimolecular star-like PAA-*b*-PS diblock copolymers as nanoreactors. First, 21 hydroxyl groups of *β*-cyclodextrin (*β*-CD) were converted to bromine groups via esterification, yielding 21-Br-*β*-CD macroinitiator[14–22] (upper central panel in Scheme 1). A series of unimolecular star-like poly(*tert*-butyl acrylate)-block-polystyrene (P*t*BA-*b*-PS) diblock copolymers with well-defined molecular weight and narrow molecular weight distribution (i.e., low polydispersity index (PDI)) of each block were then synthesized by sequential ATRP of *t*BA and St monomers using 21-Br-*β*-CD macroinitiator (upper right and lower right panels for star-like P*t*BA and P*t*BA-*b*-PS, respectively, in Scheme 1). The proton NMR (^{1}H NMR) spectra of representative star-like P*t*BA and P*t*BA-*b*-PS are shown in Figures S1 and S2 (Supporting Information). Subsequently, the inner hydrophobic P*t*BA blocks were transformed into hydrophilic PAA blocks by thoroughly hydrolyzing the *tert*-butyl groups of P*t*BA, resulting in amphiphilic star-like PAA-*b*-PS (lower central panel in Scheme 1; Figure S3, Supporting Information). As noted above, in contrast to the conventional micelles formed from self-assembly of linear amphiphilic block copolymers, each amphiphilic PAA-*b*-PS arm in star-like PAA-*b*-PS diblock copolymer is connected to the *β*-CD-based macroinitiator core. Thus, stable spherical unimolecular micelle was obtained.[14,15]

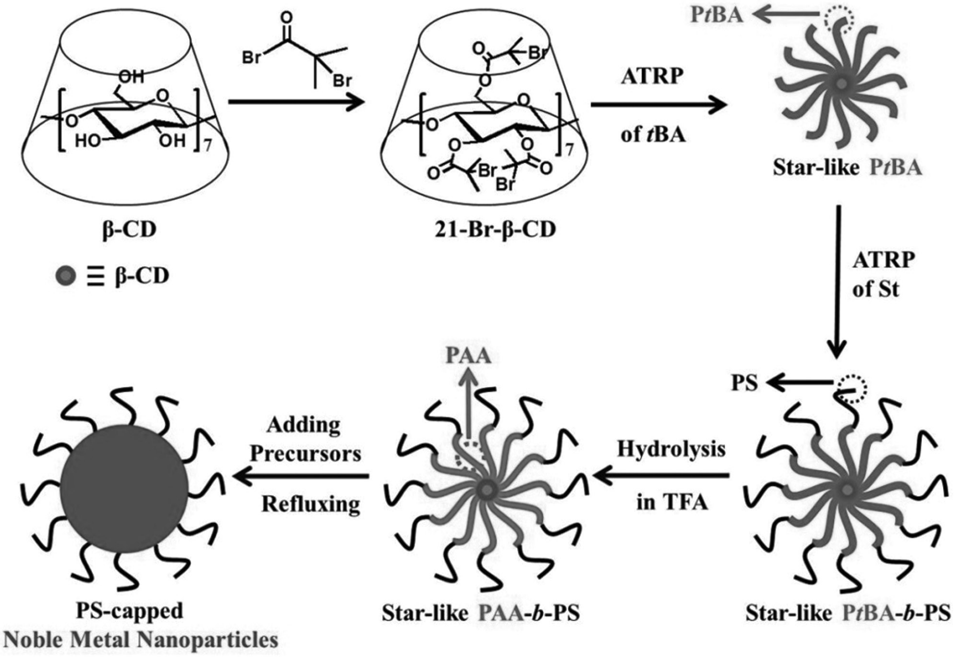

Scheme 1. Stepwise representative of synthesis of hairy plasmonic nanoparticles (e.g., PS-capped Au and Ag nanoparticles) using amphiphilic star-like PAA-*b*-PS diblock copolymers as nanoreactors (lower central panel).

The resulting amphiphilic PAA-*b*-PS diblock copolymers were exploited as nanoreactors to template the nucleation and growth of monodisperse plasmonic Au and Ag nanoparticles capped with PS chains that are originally covalently connected to inner PAA chains (i.e., PS-capped plasmonic nanoparticles; lower left panel in Scheme 1). It is interesting to note that the reaction was conducted in the mixed solvents containing *N,N*-dimethylformamide (DMF) and benzyl alcohol (BA) at DMF/BA = 9/1 ratio by volume (see the Experimental Section). In comparison to BA which is a non-solvent for PS blocks, DMF is a solvent for both PAA and PS blocks. As a result, structurally stable spherical macromolecules with well-defined shape comprising expanded inner PAA chains with collapsed outer PS chains were yielded. Subsequently, the metal-ion-containing precursors (i.e., $HAuCl_4{\bullet}3H_2O$ and $AgNO_3$, respectively) were added into the star-like PAA-*b*-PS DMF/BA solution and selectively populated in the compartment containing the expanded inner PAA chains rather than the collapsed outer PS chains. Within the PAA compartment, the metal moieties of precursors coordinated strongly with the carboxyl group of PAA blocks and grew into Au and Ag nanoparticles permanently anchored with the collapsed PS blocks in the DMF/BA mixed solvents (i.e., forming PS-capped Au and Ag nanoparticles; lower left panel in Scheme 1; see the Experimental Section). As ATRP is a living polymerization technique that produces polymer chains with well-defined molecular weight and low PDI,[23] the length of PAA blocks and in turn the shape of the resulting plasmonic nanoparticles can be strictly controlled. Moreover, by varying the ATRP time during the synthesis of each block in star-like diblock copolymer, the diameter of plasmonic nanoparticle templated within the PAA compartment and the length of PS blocks can be readily tailored. The molecular weights of PAA and PS in a series of synthesized star-like PAA-*b*-PS diblock copolymer and the corresponding diameters of PS-capped plasmonic nanoparticles are summarized in Table S1 (Supporting Information).

Figure 1 shows the representative transmission electron microscope (TEM) images of PS-capped Au and Ag nanoparticles. Uniform Au nanoparticles with the average diameters of 3.2 ± 0.1, 5.1 ± 0.2, 12.2 ± 0.5, and 18.3 ± 0.4 nm, respectively, crafted by capitalizing on four star-like PAA-*b*-PS diblock copolymers with different molecular weight of inner PAA blocks (Sample A to Sample D in Table S1, Supporting Information) were clearly evident (Figure 1a–d). The hexagonal close-pack of PS-capped Au nanoparticles (Figure 1b–d) further substantiated the high quality of nanoparticles. Similarly, Ag nanoparticles with the average diameters of 11.9 ± 0.3 nm (Figure 1e) and 18.1 ± 0.5 nm (Figure 1f) were also created using the same templates in Table S1 (Supporting Information; i.e., Sample C for 11.9 ± 0.3 nm and Sample D for 18.1 ± 0.5 nm, respectively). It is noteworthy that the size distribution of these nanoparticles is less than 5% of their average size, suggesting that they are monodisperse. The size distribution histograms for PS-capped Au and Ag nanoparticles are shown in **Figure 2**. Compared with the size of the corresponding star-like PAA measured in DMF (Figure S4 and Table S2, Supporting Information), a slight decrease in diameter of the resulting nanoparticles is due likely to the use of 9/1 DMF/BA in the reaction and the minor volume shrinking of the PAA-containing compartment during the crystallization of nanoparticles.

We also note that due to the random arrangement of the lattice planes in each nanoparticle, the brightness of Au and Ag nanoparticles varied in TEM images (Figure 1).[24] Representative high-resolution TEM images of 3 nm (Figure 1a)

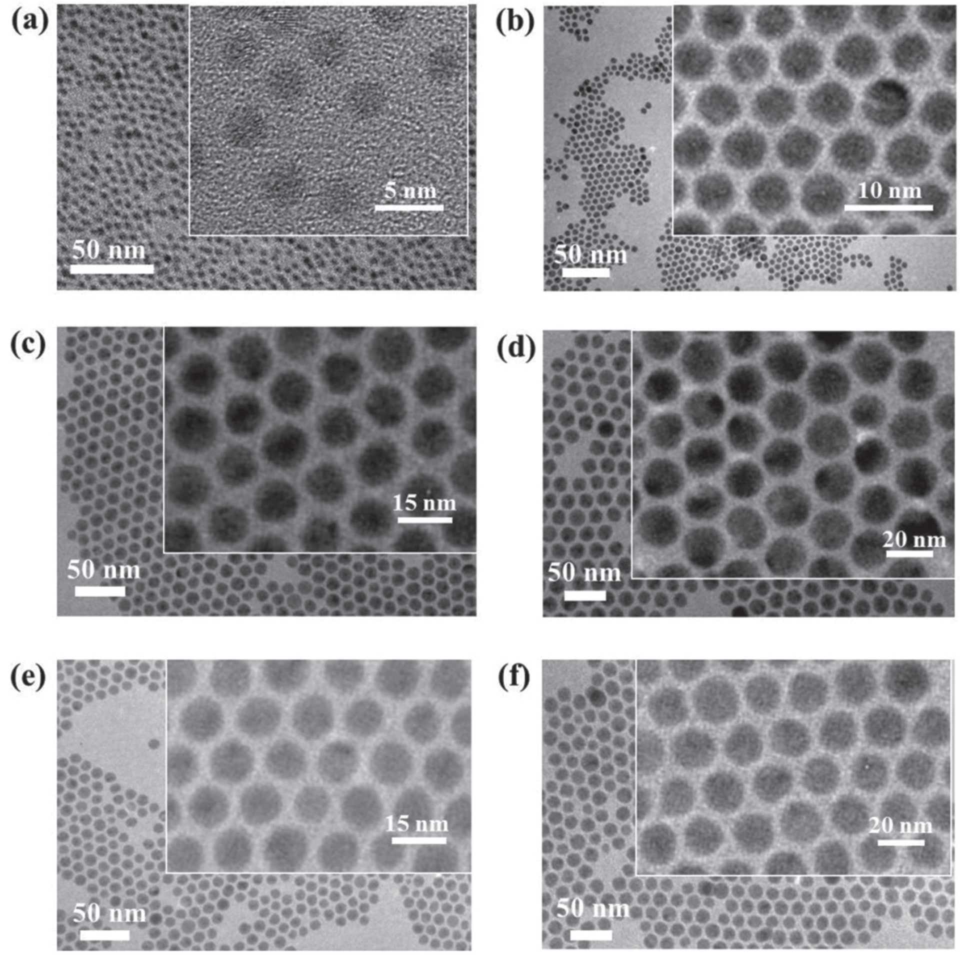

Figure 1. TEM images of monodisperse PS-capped noble metal nanoparticles crafted using amphiphilic star-like PAA-*b*-PS diblock copolymers as nanoreactors. PS-capped Au nanoparticles with diameters of a) 3.2 ± 0.1 nm, b) 5.1 ± 0.2 nm, c) 12.2 ± 0.5 nm, and d) 18.3 ± 0.4 nm. PS-capped Ag nanoparticles with diameters of e) 11.9 ± 0.3 nm and f) 18.1 ± 0.5 nm.

and 18 nm (Figure 1d) Au nanoparticles showed that they are highly crystalline with a lattice spacing of ca. 2.4 Å, which is in good agreement with the (111) interplanar distance of the face-centered cubic (fcc) structure of Au (**Figure 3**).

In contrast to rather weak physical adsorption or chemical coupling of ligands on the nanoparticle surface in previous works, the surface of plasmonic nanoparticles was reliably and permanently capped with soft PS chains enabled by the pre-existing strong covalent bonding between PAA and PS chains in star-like PAA-*b*-PS templates. Interestingly, single-layer and two-layer assemblies (Figure S5, Supporting Information) of PS-capped Au nanoparticles were observed (D = 12.2 ± 0.5 nm; top right and bottom right, respectively, in **Figure 4**). Obviously, the formation of these assemblies was driven by the minimization of surface energy of monodisperse PS-capped Au nanoparticles through reducing the exposed surface areas during the solvent (i.e., toluene; these PS-capped Au nanoparticles were re-dissolved in toluene after synthesis) evaporation. In order to examine the PS chains situated on the Au nanoparticle surface, the TEM grid can be exposed to RuO_4 vapor to preferentially stain the PS chains, yielding a dark appearance. The representative TEM image of PS-capped Au nanoparticles with the Au core diameter of 12 nm and PS shell thickness of 4 nm (Sample C in Table S1, Supporting Information) stained by RuO_4 vapor is shown as an inset in Figure 4. Quite intriguingly, a layer of PS chains covered on the surface of Au nanoparticle was seen, and the interface between Au nanoparticle and PS shell is intimate (darker Au core and relatively light PS shell in inset). It is notable that despite the relatively close molecular weights of PAA and PS blocks (Sample C in Table S1, Supporting Information), the smaller thickness of PS shell compared to Au core suggested the collapsed chain conformation of PS blocks on the surface of Au nanoparticle. As a direct consequence, PS-capped Au nanoparticles can be readily dissolved in nonpolar solvents with a superior long-term stability (**Figure 5**). No precipitation was observed for months. Moreover, the superior stability of the PS-capped Au nanoparticles compared with oleylamine-capped Au nanoparticles was examined by employing UV irradiation as shown in **Figure 6**. The size and shape of PS-capped Au nanoparticles after irradiation (Figure 6a) were the same as those prior to irradiation (Figure 1) due to the presence of intimately linked PS chains. However, the spherical oleylamine-capped Au nanoparticles (Figure S6, Supporting Information) aggregated heavily with irregular shapes after

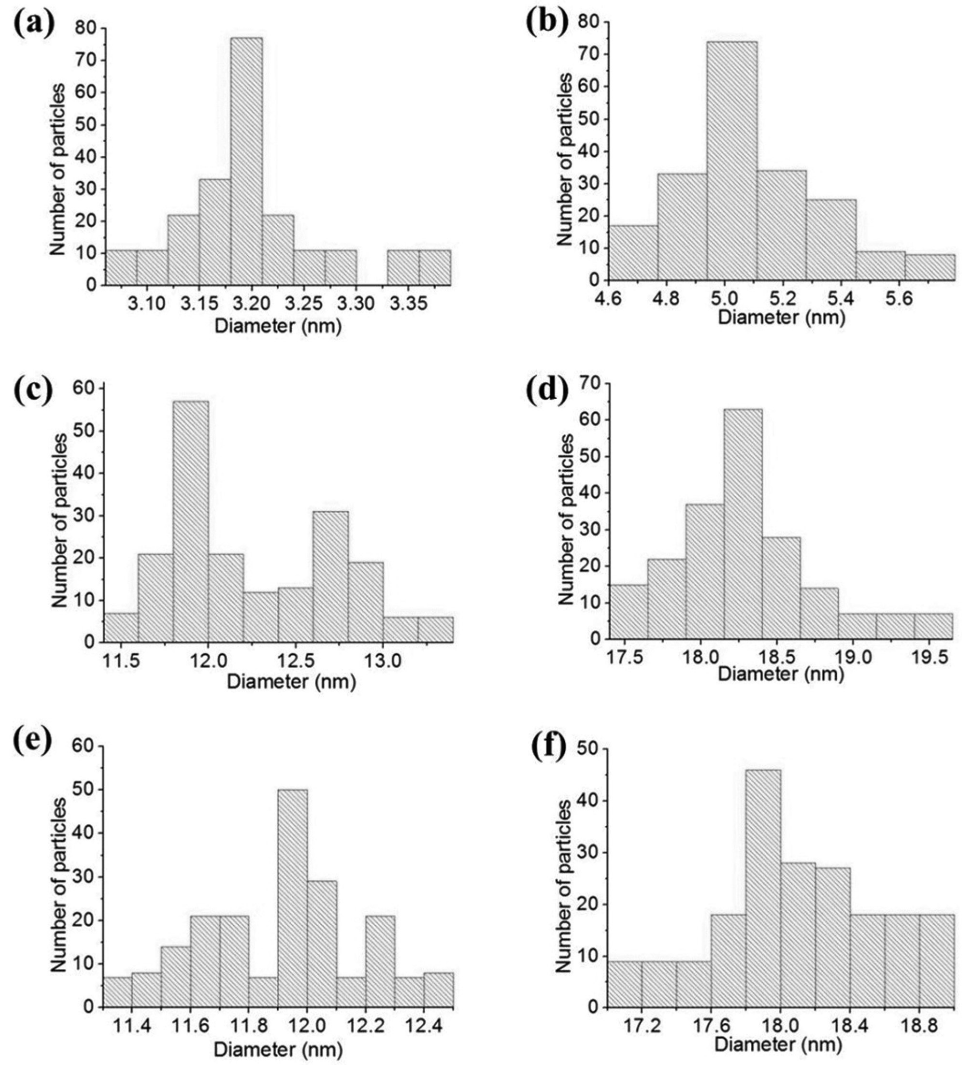

Figure 2. Histograms of the size distribution of randomly selected 200 nanoparticles for TEM images in Figure 1. PS-capped Au nanoparticles with diameters of a) 3.2 ± 0.1 nm, b) 5.1 ± 0.2 nm, c) 12.2 ± 0.5 nm, and d) 18.3 ± 0.4 nm. PS-capped Ag nanoparticles with diameters of e) 11.9 ± 0.3 nm and f) 18.1 ± 0.5 nm.

irradiation (Figure 6b) owing to the UV irradiation-induced desorption of ligands.[5] Clearly, the PS-capped Au nanoparticles were much more stable than those prepared by the conventional technique.

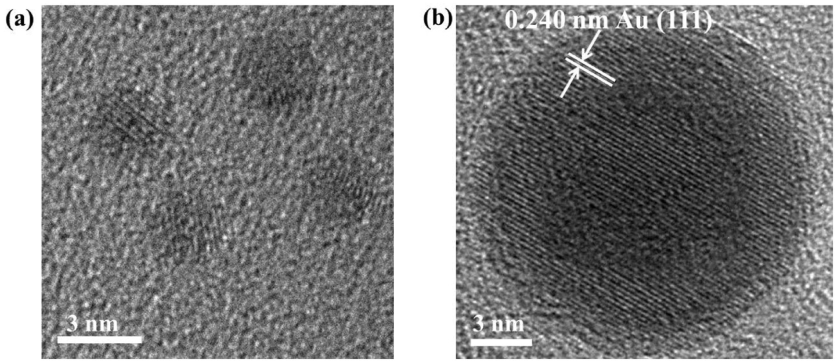

Figure 3. HRTEM images of Au nanoparticles permanently capped with PS chains on the surface. The diameters of Au core are a) 3 nm and b) 18 nm, respectively.

Typical X-ray diffraction (XRD) patterns of PS–capped plasmonic nanoparticles are shown in **Figure 7**. The peaks from PS-capped Au nanoparticles at scattering angle, 2θ of 37.81°, 43.96°, 64.23°, 77.19°, and 81.42° correspond to the diffraction from the (111), (200), (220), (311), and (222) crystal planes of fcc Au, respectively (Figure 7a). The PS-capped Ag nanoparticles showed the similar XRD pattern (Figure 7b). Clearly, the XRD measurements suggested that Au and Ag nanoparticles formed by the nanoreactor strategy were crystalline.

The SPR properties of PS-capped Au and Ag nanoparticles as a function of nanoparticle size were then systematically examined. The UV–vis absorption spectra of PS-capped Au nanoparticles and Ag nanoparticles in toluene are shown in **Figure 8**. Compared with

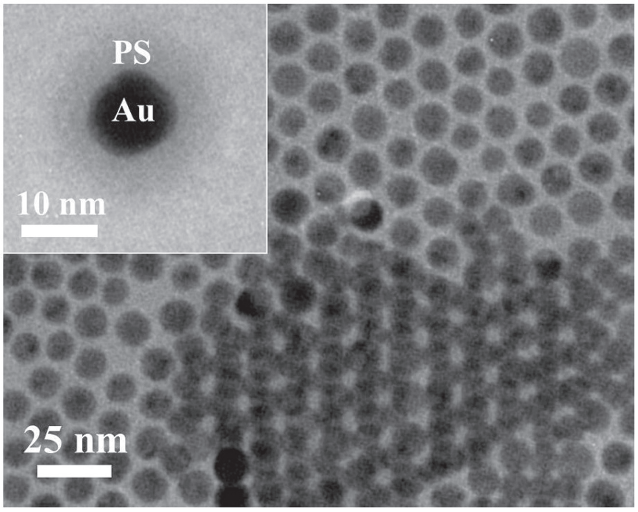

Figure 4. TEM image of single-layer (upper right) and two-layer (lower right) assemblies of 12 nm Au nanoparticles intimately and permanently capped with PS chains on the surface. A layer of PS "hairs" on the surface of Au nanoparticles obtained after being stained by RuO_4 vapor is clearly evident as shown in the inset.

oleylamine-capped Au nanoparticles, the red-shift of SPR peak position of PS-capped Au nanoparticles suggested the existence of PS shell due to the higher refractive index of PS than oleylamine (Figure S7, Supporting Information). As the diameter of Au nanoparticles increased, the intensity of the characteristic SPR peak increased associated with a marginal red-shift in the peak position and a decreased full-width-at-half-maximum (FWHM) (Figure 8a). These observations correlated well with the reports in literature and can be attributed to more electrons in larger Au nanoparticles and non-negligible electromagnetic retardation.[25] Similarly, for PS-capped Ag nanoparticles, as the size increased from 11.9 ± 0.3 nm to 18.1 ± 0.5 nm, the characteristic SPR peak at around 420 nm exhibited an increase in intensity and a narrowing in FWHM (Figure 8b), which agreed well with the reports in literature.[26] It is worth noting that such good agreements between our work and previous studies on plasmonic absorption behaviors of Au and Ag nanoparticles corroborated that our nanoreactor strategy renders the crafting of high-quality noble metal nanoparticles that possess as good plamonic properties as those prepared by other means.[25,26] According to Mie theory, compared with the

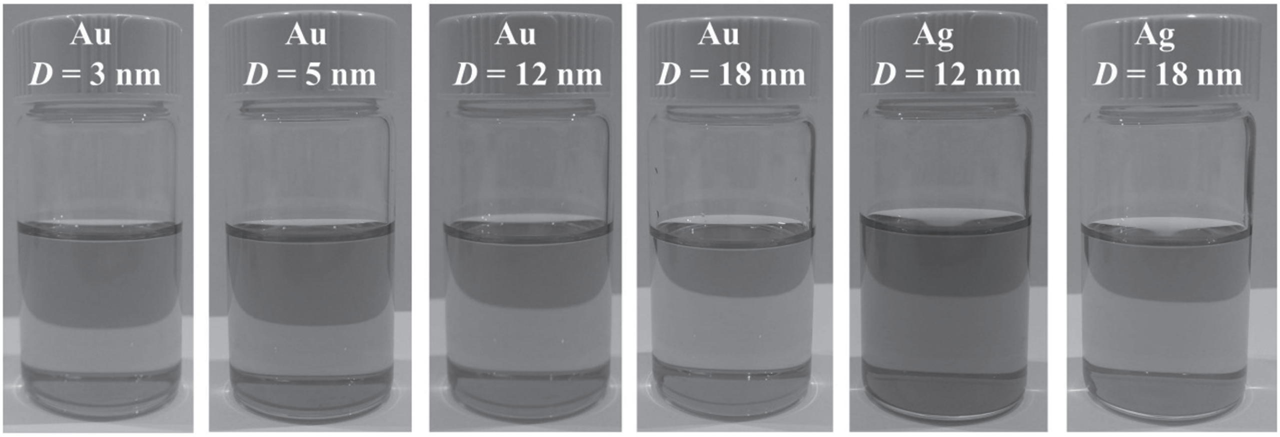

Figure 5. Digital images of PS-capped noble metal nanoparticles that are well dissolved in toluene.

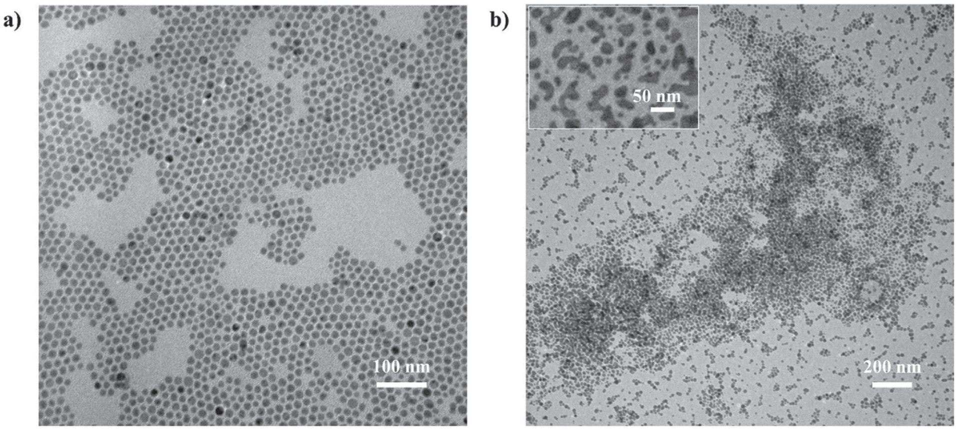

Figure 6. TEM images of a)18 nm PS-capped Au nanoparticles after irradiation of 254 nm UV light for 12 h and b) 18 nm oleylamine-capped Au nanoparticles after irradiation of 254 nm UV light for 1 h.

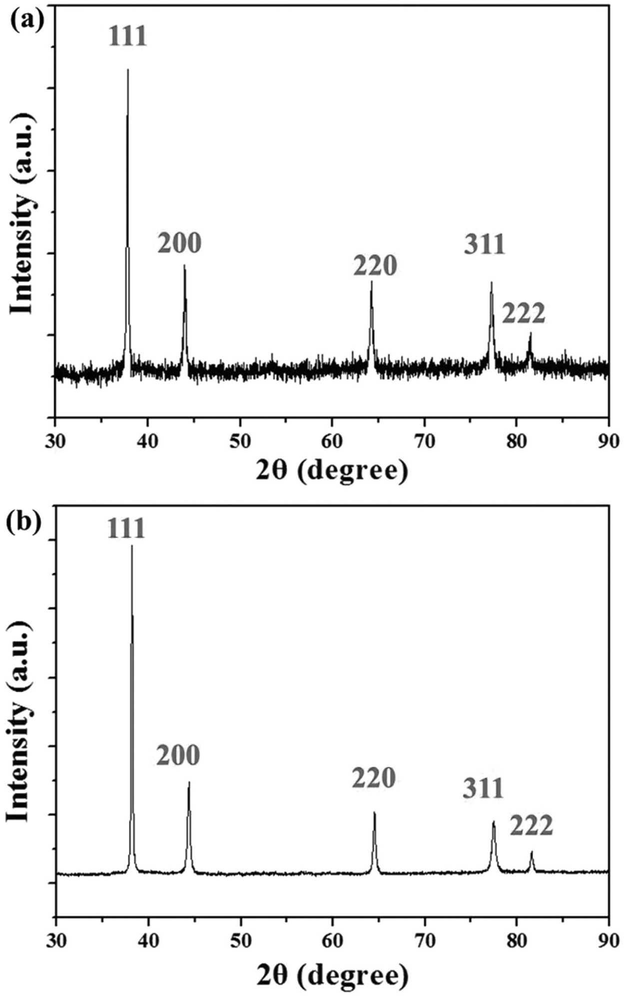

Figure 7. XRD patterns of a) PS-capped Au nanoparticles, and b) PS-capped Ag nanoparticles.

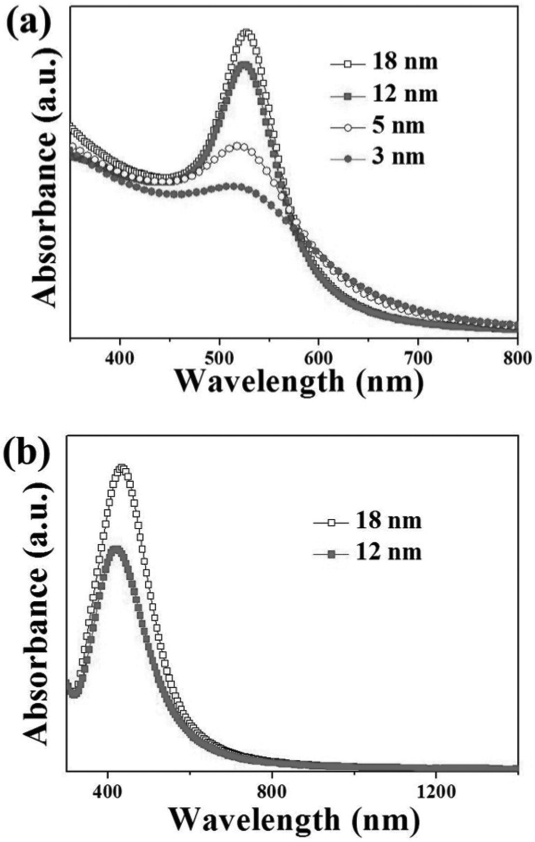

Figure 8. UV–vis spectra of a) PS-capped Au nanoparticles with diameters of 3.2 ± 0.1, 5.1 ± 0.2, 12.2 ± 0.5, and 18.3 ± 0.4 nm, respectively, and b) PS-capped Ag nanoparticles with diameters of 11.9 ± 0.3 and 18.1 ± 0.5 nm, respectively.

wavelength of light, nanoparticle with a finite diameter (typically below 50 nm) responds as an induced dipole resulting from the electric field of incident light when being irradiated with light (i.e., dipole approximation). Based on this dipole approximation, one most primitive theoretical model for the optical spectrum of noble metal nanoparticles is given as follows[27]

$$E(\lambda)=\frac{24\pi^2NR^3\varepsilon_{\text{out}}^{3/2}}{\lambda\ln(10)}\left[\frac{\varepsilon_i(\lambda)}{\left(\varepsilon_r(\lambda)+\chi\varepsilon_{\text{out}}\right)^2+\varepsilon_i(\lambda)^2}\right] \tag{1}$$

E(λ) is the extinction (i.e., the sum of absorption and scattering cross-section), N is the areal density of nanoparticles, R is the radius of spherical noble metal nanoparticles, ε_{out} is the dielectric constant of the surrounding medium (assumed to be frequency-independent), λ is the wavelength of the absorbing radiation, ε_i and ε_r represent the imaginary and real portions of the dielectric function of nanoparticle, ε ($\varepsilon(\omega) = \varepsilon_i(\omega) + i\varepsilon_r(\omega)$), where ω is the angular frequency of light), and the value of χ describing the aspect ratio of nanoparticle is 2 for sphere.[28] From this model, it is clear that the experimental optical spectrum of noble metel nanoparticles depends on their radius R and the dielectric function ε.

When $2R$ is less than electronic mean-free path (≈50 nm for Au and Ag), the scattering of free electrons on the surface affects their responses to optical excitation, thereby resulting in depolarization.[29] The spontaneous emission of radiation from the induced dipole, which increases rapidly with the nanoparticle size, causes a radiative damping.[30] Both depolarization and radiative damping lead to the red-shift of the SPR peak as the nanoparticle size increases.[30] Considering the intrinsic size effect that includes the effect of free electrons, surface damping, and interband transitions, dielectric function $\varepsilon(\omega)$ described above is thus modified based on Drude model to reflect the size-dependent effect and given in the following[31]

$$\varepsilon(\omega,R)=\varepsilon_{\text{bulk}}+\frac{\omega_P^2}{\omega^2+i\omega\gamma_D}-\frac{\omega_P^2}{\omega^2+i\omega\left(\gamma_D+\frac{AV_F}{R}\right)} \tag{2}$$

$\varepsilon_{\text{bulk}}$, ω_P, γ_D, V_F and R are the bulk dielectric constant, the plasma frequency, the bulk damping constant, the Fermi velocity of electron cloud, and the radius of spherical noble metal nanoparticles, respectively. After solving the dielectric function $\varepsilon(\omega, R)$, the optical spectrum of noble metal nanoparticles can be simulated by numerical methods such as discrete dipole approximation. The simulation results reported in literature have also shown the same plasmonic characteristics (i.e., an increase in intensity, a decrease in FWHM, and a slight red-shift as the nanoparticle size increases) as seen in our experiments.[30]

3. Conclusion

In summary, we demonstrate in-situ precision synthesis of hairy plasmonic Au and Ag nanoparticles with tailored sizes and compositions by capitalizing on amphiphilic star-like PAA-*b*-PS diblock copolymers as nanoreactors. These nanoreactors were synthesized via sequential ATRP of *t*BA and St from the *β*-cyclodextrin-based macroinitiator, followed by subsequent hydrolysis of inner P*t*BA blocks. Intriguingly, these hairy plasmonic nanoparticles can be regarded as hard/soft core/shell nanoparticles composed of monodisperse plasmonic nanoparticle core intimately and permanently capped with PS shell of uniform length. By simply varying the molecular weights of inner hydrophilic PAA blocks and outer hydrophobic PS blocks in star-like PAA-*b*-PS nanoreactors, the diameter of plasmonic nanoparticles and the thickness of PS shell, respectively, can be accurately controlled. It is interesting to note that the ability to tune the length of PS blocks permanently situated on the surface of plasmonic nanoparticles render the deliberate variation of distance between adjacent plasmonic nanoparticles for enhanced SERS.[32] Furthermore, hairy nanoparticles of this kind can be homogeneously dispersed in PS matrix, PS-derived polymer matrix (for example, phenyltrinetoxysilane via forming a homogeneous hybrid due to the *π*–*π* interaction between phenyl groups), or PS blocks in PS-containing linear diblock or triblock copolymers[33] that virtually eliminating enthalpic interaction of nanoparticles with the host matrix.[34] Moreover, the PS shell (i.e., PS "hair") can be further carbonized under inert atmosphere to yield conductive carbon-coated plasmonic nanoparticles.[35,36] As the carbon coating promotes the charge transfer, such carbon-coated plasmonic nanoparticles may find promising applications in biosensors[37] and solar cells.[17] This will be the subject of future study. Finally, although noble metals were chosen as examples to demonstrate the effectiveness of our nanoreactor strategy in producing monodisperse hairy nanoparticles, we envision that given a variety of precursors that are amenable to such nanoreactor-based reactions, this strategy offer great potential to create a myriad of other hairy nanoparticles with well-controlled dimensions and compositions for applications in energy conversion and storage, catalysis, nanotechnology, plasmonic devices, surface plasmon-based biosensing and bioimaging.

4. Experimental Section

Materials: 2-Bromoisobutyryl bromide (98%), *N,N,N′,N″,N″*-pentamethyldiethylene triamine (PMDETA, 99%), anhydrous 1-methyl-2-pyrrolidinone (NMP, 99.5%), trifluoroacetic acid (TFA, 99.9%), gold(III) chloride trihydrate ($HAuCl_4•3H_2O$, ≥99.9%), silver nitrate ($AgNO_3$, ≥99.0%), oleylamine (technical grade, 70%), and *tert*-butylamine borane (TBAB, 97%) were purchased from Sigma-Aldrich, and used as received. *β*-cyclodextrin (*β*-CD, Sigma-Aldrich) was dried at 80 °C under vacuum overnight prior to use. CuBr (98%, Sigma-Aldrich) was stirred in acetic acid overnight, washed with ethanol and diethyl ether, respectively, and dried under vacuum. *t*BA (Sigma-Aldrich, 98%), anisole (TCI America, 99.0%), methyl ethyl ketone (MEK, Fisher Scientific, 99.9%) and DMF (Fisher Scientific, 99.9%) were dried over calcium hydride (CaH_2) and distilled under reduced pressure prior to use. Styrene (St, Sigma-Aldrich, ≥99%) was washed with 10% NaOH aqueous solution and water successively, dried over anhydrous $MgSO_4$ and CaH_2 sequentially, and distilled under reduced pressure. All other reagents were purified by common purification procedures.

Synthesis of Multiarm, Star-Like Poly(tert-Butyl Acrylate) (PtBA) Terminated with Bromine End Groups (Star-Like PtBA-Br): Heptakis[2,3,6-tri-*O*-(2-bromo-2-methylpropionyl)]-*β*-cyclodextrin (denoted 21Br-*β*-CD) was prepared according to previous work.[14,15] Using 21Br-*β*-CD as the macroinitiator, star-like P*t*BA-Br was synthesized by ATRP of *t*BA monomers in MEK. Typically, CuBr (35.0 mg), PMDETA (85.0 mg), 21Br-*β*-CD (50 mg), *t*BA (21 mL), and MEK (21 mL) were mixed in an argon purged ampule and degassed by three freeze-pump-thaw cycles. The ampule was sealed and dipped in an oil bath at 60 °C. After a certain desired time, the reaction was quenched by dipping the ampule in liquid N_2. The mixture was then diluted with THF and passed through a column of neutral alumina to remove the catalyst and subsequently purified by fractional precipitation with methanol/water (v/v = 1/1) as the precipitator. The product was dried at 40 °C under vacuum for 2 d.

Synthesis of Multiarm, Star-Like Poly(tert-Butyl Acrylate)-block-Polystyrene (PtBA-b-PS) Diblock Copolymer: A typical ATRP reaction was performed as follows. The reaction mixture at styrene: star-like P*t*BA (i.e., Br in P*t*BA macroinitiator): copper bromide: PMDETA = 800: 1: 1: 2 (molar ratio) in anisole (1 g St in 1 mL solvent) was placed in a argon purged ampule and degassed by three freeze-pump-thaw cycles. The polymerization was performed at 90 °C and quenched by dipping the ampule in liquid N_2 after a certain desired time. The crude product was diluted with THF and passed through a neutral alumina column to remove the catalyst and purified by fractional precipitation with methanol/water (v/v = 1/1) as the precipitator. The product, multiarm, star-like P*t*BA-*b*-PS was dried at 40 °C under vacuum for 2 d.

Synthesis of Multiarm, Star-Like Poly(Acrylic Acid)-block-Polystyrene (PAA-b-PS) Diblock Copolymer by Hydrolysis: By hydrolyzing *tert*-butyl ester groups of P*t*BA blocks in P*t*BA-*b*-PS diblock copolymers, amphiphilic star-like PAA-*b*-PS diblock copolymers were created. Briefly, star-like P*t*BA-*b*-PS (0.4 g) was dissolved in $CHCl_3$ (40 mL), followed by the addition of TFA (3 mL). The reaction mixture was stirred at room temperature for 24 h. After the hydrolysis, the resulting amphiphilic star-like PAA-*b*-PS diblock copolymer was gradually precipitated in $CHCl_3$. The final product was washed with $CHCl_3$, and thoroughly dried under vacuum at 40 °C.

Synthesis of PS-Capped Au Nanoparticles: By capitalizing on star-like PAA-*b*-PS diblock copolymers as nanoreactors, the strong coordination interaction between Au precursors ($HAuCl_4•3H_2O$) that are selectively partitioned in the space occupied by inner hydrophilic PAA blocks of star-like PAA-*b*-PS diblock copolymers and the carboxyl groups of PAA led to the nucleation and growth of PS-capped Au nanoparticles. In a typical procedure, star-like PAA-*b*-PS (10 mg) was dissolved in mixed solvents containing DMF

(9 mL) and BA (1 mL) at room temperature, followed by the addition of $HAuCl_4 \bullet 3H_2O$ as precursor with TBAB as reducer. The molar ratio of acrylic acid (AA) units in PAA blocks to precursor was set at 1:10 in order to maximize the loading of precursors into the PAA compartment noted above. Compared to BA which is a poor solvent for the outer PS blocks, DMF is a good solvent for both inner PAA and outer PS blocks. Thus, the addition of BA resulted in the formation of structurally stable, sphere-shaped macromolecule composed of inner expanded PAA chain and outer collapsed PS chains. Meanwhile, the precursors $HAuCl_4 \bullet 3H_2O$ were preferentially incorporated in the compartment containing the inner PAA blocks in the mixed solvents of DMF/BA. As noted above, $HAuCl_4 \bullet 3H_2O$ coordinated with the carboxyl groups of PAA blocks within the compartment, leading to the nucleation and growth of Au nanoparticles and eventually forming Au nanoparticles fully occupied the PAA compartment with PS blocks capped on the surface. The solution was stirred under argon at room temperature to ensure that all the chemicals were completely dissolved and then immersed in an oil bath at 60 °C under argon for 2 h. The solution was then purified by ultracentrifugation with toluene as solvent and ethanol as precipitant several times to remove remaining precursors and mixed solvents, yielding Au nanoparticles intimately and stably capped with PS.

Synthesis of PS-Capped Ag Nanoparticles: Similarly, PS-capped Ag nanoparticles were synthesized using star-like PAA-*b*-PS diblock copolymers as nanoreactors. The mixed solvent and their ratio as well as the formation mechanism were the same as the synthesis of PS-capped Au nanoparticles described above. The precursors and reducer used were $AgNO_3$ and ethanol, respectively. The molar ratio of AA units in PAA blocks to precursor was set at 1:10 in order to maximize the loading of precursors into the PAA compartment noted above. Likewise, after all the chemicals in the mixture solution stirred under argon at room temperature were completely dissolved, it was immersed in an oil bath at 100 °C under argon for 10 h. The same purification procedure as PS-capped Au nanoparticles was taken to yield Ag nanoparticles intimately and stably capped with PS.

Synthesis of Oleylamine-Capped Au Nanoparticles: Oleylamine-capped Au nanoparticles with a diameter of 18.1 ± 4.2 nm were prepared by following the method previously reported.[38] Briefly, $HAuCl_4 \bullet 3H_2O$ (24 mg) and oleylamine (1.2 mL) were dissolved in toluene (1 mL). This mixture was added to a boiling solution of oleylamine (2.09 mL) and toluene (49 mL) to start the reaction. After 2 h, the solution was purified by ultracentrifugation several times with toluene as solvent and ethanol as precipitant to remove unreacted precursors and mixed solvents, yielding oleylamine-capped Au nanoparticles.

Characterizations: The number average molecular weight, M_n, and polydispersity index, PDI, were measured by gel permeation chromatography (GPC) equipped with an LC-20AD HPLC pump and a refractive index detector (RID-10A, 120V) at 35 °C. A series of monodisperse polystyrene were used as the standard samples with THF as the eluent at a flow rate of 1.0 mL min^{-1} to calibrate the GPC. All proton nuclear magnetic resonance (^1H NMR) spectra of star-like P*t*BA and star-like P*t*BA-*b*-PS in $CDCl_3$ and star-like PAA-*b*-PS in d_7-DMF were recorded using a Varian VXR-300 spectroscope.

The size and morphology of PS-capped Au and Ag nanoparticles were examined by TEM (JEOL 100; operated at 100 kV) and high-resolution TEM (HRTEM, TECNAIG2 F30; operated at 300 kV). TEM samples were prepared by dropping nanoparticle solution onto a carbon-coated copper TEM grid (300 mesh) and evaporating toluene under ambient condition. In order to observe the PS shell on the surface of nanoparticles, TEM samples were subsequently stained with RuO_4 vapor. The plasmonic properties of nanoparticles were measured by UV–vis spectroscopy (Varian; UV–vis–NIR spectrophotometer, Cary 5000). Mercury low pressure UV lamp at 254 nm (4 W) was used for the irradiation of dilute solution containing PS-capped Au or oleylamine-capped Au nanoparticles. Dynamic light scattering data was acquired using laser light scattering spectrometer (Malvern Autosizer 4700) at 25 °C. The crystalline structures of nanoparticles were evaluated by XRD (X'pert PRO, Netherlands).

Supporting Information

Supporting Information is available from the Wiley Online Library or from the author.

Acknowledgment

Y.C. and Y.J.Y. contributed equally to this work. Y.C. and G.Z. gratefully acknowledge the financial support from the China Scholarship Council. This work was supported by the Air Force Office of Scientific Research (FA9550-16-1-0187) and the National Science Foundation (CMMI 1562075, Z.L.).

---

[1] P. K. Jain, X. Huang, I. H. El-Sayed, M. A. El-Sayed, *Acc. Chem. Res.* **2008**, *41*, 1578.
[2] T. Ishida, M. Haruta, *Angew. Chem., Int. Ed.* **2007**, *46*, 7154.
[3] L. Brus, *Acc. Chem. Res.* **2008**, *41*, 1742.
[4] J. Park, J. Joo, S. G. Kwon, Y. Jang, T. Hyeon, *Angew. Chem., Int. Ed.* **2007**, *46*, 4630.
[5] D. Ling, M. J. Hackett, T. Hyeon, *Nano Today* **2014**, *9*, 457.
[6] R. A. Álvarez-Puebla, R. Contreras-Cáceres, I. Pastoriza-Santos, J. Pérez-Juste, L. M. Liz-Marzán, *Angew. Chem., Int. Ed.* **2009**, *48*, 138.
[7] B. Wang, B. Li, B. Zhao, C. Y. Li, *J. Am. Chem. Soc.* **2008**, *130*, 11594.
[8] J. Chai, D. Wang, X. Fan, J. M. Buriak, *Nat. Nanotechnol.* **2007**, *2*, 500.
[9] B. Zhao, W. J. Brittain, *Prog. Polym. Sci.* **2000**, *25*, 677.
[10] G. Riess, *Prog. Polym. Sci.* **2003**, *28*, 1107.
[11] J. Rodríguez-Hernández, F. Chécot, Y. Gnanou, S. Lecommandoux, *Prog. Polym. Sci.* **2005**, *30*, 691.
[12] S. Darling, *Prog. Polym. Sci.* **2007**, *32*, 1152.
[13] R. M. Crooks, M. Zhao, L. Sun, V. Chechik, L. K. Yeung, *Acc. Chem. Res.* **2001**, *34*, 181.
[14] X. Pang, L. Zhao, M. Akinc, J. K. Kim, Z. Lin, *Macromolecules* **2011**, *44*, 3746.
[15] X. Pang, L. Zhao, C. Feng, Z. Lin, *Macromolecules* **2011**, *44*, 7176.
[16] X. Pang, L. Zhao, W. Han, X. Xin, Z. Lin, *Nat. Nanotechnol.* **2013**, *8*, 426.
[17] D. Zheng, X. Pang, M. Wang, Y. He, C. Lin, Z. Lin, *Chem. Mater.* **2015**, *27*, 5271.

[18] H. Xu, Y. Xu, X. Pang, Y. He, J. Jung, H. Xia, Z. Lin, *Sci. Adv.* **2015**, *1*, e1500025.
[19] H. Xu, X. Pang, Y. He, M. He, J. Jung, H. Xia, Z. Lin, *Angew. Chem., Int. Ed.* **2015**, *54*, 4636.
[20] D. Yang, X. Pang, Y. He, Y. Wang, G. Chen, W. Wang, Z. Lin, *Angew. Chem., Int. Ed.* **2015**, *54*, 12091.
[21] M. He, X. Pang, X. Liu, B. Jiang, Y. He, H. Snaith, Z. Lin, *Angew. Chem., Int. Ed.* **2016**, *55*, 4280.
[22] M. Wang, X. Pang, D. Zheng, Y. He, L. Sun, C. Lin, Z. Lin, *J. Mater. Chem. A* **2016**. *4*, 7190.
[23] K. Matyjaszewski, N. V. Tsarevsky, *Nat. Chem.* **2009**, *1*, 276.
[24] T. Shimizu, T. Teranishi, S. Hasegawa, M. Miyake, *J. Phys. Chem. B* **2003**, *107*, 2719.
[25] K. A. Willets, R. P. Van Duyne, *Annu. Rev. Phys. Chem.* **2007**, *58*, 267.
[26] X. Wang, J. Zhuang, Q. Peng, Y. Li, *Nature* **2005**, *437*, 121.
[27] U. Kreibig, M. Vollmer*Optical Properties of Metal Clusters*, Springer, Berlin **1995**.
[28] S. Link, M. A. El-Sayed, *J. Phys. Chem. B* **1999**, *103*, 8410.
[29] O. Sqalli, M.-P. Bernal, P. Hoffmann, F. Marquis-Weible, *Appl. Phys. Lett.* **2000**, *76*, 2134.
[30] K. L. Kelly, E. Coronado, L. L. Zhao, G. C. Schatz, *J. Phys. Chem. B* **2003**, *107*, 668.
[31] C. Noguez, *J. Phys. Chem. C* **2007**, *111*, 3806.
[32] Y. C. Cao, R. Jin, C. A. Mirkin, *Science* **2002**, *297*, 1536.
[33] X. Pang, Y. He, B. Jiang, J. Iocozzia, L. Zhao, H. Guo, J. Liu, M. Akinc, N. Bowler, X. Tan, Z. Lin, *Nanoscale* **2013**, *5*, 8695.
[34] R. F. Ziolo, E. P. Giannelis, B. A. Weinstein, M. P. O'Horo, B. N. Ganguly, V. Mehrotra, M. W. Russell, D. R. Huffman, *Science* **1992**, *257*, 219.
[35] W. C. Mai, B. Sun, L. Y. Chen, F. Xu, H. Liu, Y. R. Liang, R. W. Fu, D. C. Wu, K. Matyjaszewski, *J. Am. Chem. Soc.* **2015**, *137*, 13256.
[36] D. C. Wu, Z. H. Li, M. J. Zhong, T. Kowalewski, K. Matyjaszewski, *Angew. Chem., Int. Ed.* **2014**, *53*, 3957.
[37] L. Wang, J. Bai, X. Bo, X. Zhang, L. Guo, *Talanta* **2011**, *83*, 1386.
[38] O. C. Compton, F. E. Osterloh, *J. Am. Chem. Soc.* **2007**, *129*, 7793.

Received: August 23, 2016
Revised: September 17, 2016